Journal of Electrochemistry

Volume 29 | Issue 9

2023-09-28

Asymmetric Electrode-Electrolyte Interfaces for High-Performance Rechargeable Lithium-Sulfur Batteries

Jia Chou

Ya-Hui Wang

Wen-Peng Wang

Sen Xin
CAS Key Laboratory of Molecular Nanostructure and Nanotechnology, CAS Research/Education Center for Excellence in Molecular Sciences, Institute of Chemistry, Chinese Academy of Sciences (CAS), Beijing 100190, China;University of Chinese Academy of Sciences, Beijing 100049, China, xinsen08@iccas.ac.cn

Yu-Guo Guo
CAS Key Laboratory of Molecular Nanostructure and Nanotechnology, CAS Research/Education Center for Excellence in Molecular Sciences, Institute of Chemistry, Chinese Academy of Sciences (CAS), Beijing 100190, China; University of Chinese Academy of Sciences, Beijing 100049, China, ygguo@iccas.ac.cn

Recommended Citation

Jia Chou, Ya-Hui Wang, Wen-Peng Wang, Sen Xin, Yu-Guo Guo. Asymmetric Electrode-Electrolyte Interfaces for High-Performance Rechargeable Lithium-Sulfur Batteries[J]. *Journal of Electrochemistry*, 2023 , 29(9): 2217009.
DOI: 10.13208/j.electrochem.2217009
Available at: https://jelectrochem.xmu.edu.cn/journal/vol29/iss9/1

PERSPECTIVE

Asymmetric Electrode-Electrolyte Interfaces for High-Performance Rechargeable Lithium-Sulfur Batteries

Jia Chou [a,b], Ya-Hui Wang [a,b], Wen-Peng Wang [a], Sen Xin [a,b,*], Yu-Guo Guo [a,b,*]

[a] CAS Key Laboratory of Molecular Nanostructure and Nanotechnology, CAS Research/Education Center for Excellence in Molecular Sciences, Institute of Chemistry, Chinese Academy of Sciences (CAS), Beijing 100190, China
[b] University of Chinese Academy of Sciences, Beijing 100049, China

Abstract

With a high cell-level specific energy and a low cost, lithium-sulfur (Li-S) battery has been intensively studied as one of the most promising candidates for competing the next-generation energy storage campaign. Currently, the practical use of Li-S battery is hindered by the rapidly declined storage performance during battery operation, as caused by irreversible loss of electroactive sulfide species at the cathode, dendrite formation at the anode and parasitic reactions at the electrode-electrolyte interface due to unfavorable cathode-anode crosstalk. In this perspective, we propose to stabilize the Li-S electrochemistry, and improve the storage performance of battery by designing asymmetric electrode-electrolyte interfaces that helps to simultaneously address the differentiated issues at both electrodes and facilitate charge transfer in the electrode/electrolyte and across the interfaces. The strategies discussed would shed lights on reasonable design of battery interfaces towards realization of high-performance Li-S batteries.

Keywords: Lithium-sulfur battery; Lithium metal anode; Sulfur cathode; Electrode-electrolyte interface

1. Introduction

Among advanced rechargeable batteries, Li-S battery has attained much attention in terms of being applied to emerging fields including grids and automobiles. It couples S cathode and Li metal anode, and both electrodes present theoretical specific capacities (S: 1675 $mAh \cdot g^{-1}$; Li: 3860 $mAh \cdot g^{-1}$), an order of magnitude higher than the electrode materials of traditional Li-ion batteries (e.g., $LiFePO_4$: 170 $mAh \cdot g^{-1}$ and graphite: 372 $mAh \cdot g^{-1}$). As a result, the Li-S battery is capable to offer six times higher energy density than the Li-ion batteries (LIBs). Whereas, the practical application of Li-S battery is also hindered by both the challenges of S cathode and Li metal anode [1−4].

Different from intercalation-based lithium-ion batteries, S cathode follows a two-electron conversion chemistry $1/8S_8 + 2Li \leftrightarrow Li_2S$. In the lithiation and delithiation reactions, the sulfur molecules would experience a stepwise transformation of solid-liquid-solid state. With high solubility, the intimidate products, high-order polysulfides (e.g., Li_2S_x, $x = 4−8$), tend to be dissolved in ether electrolyte, and shuttled from the cathode to the anode under the electric field, and finally deposited on the Li anode, which passivate the surface. Except for the dissolution and shuttle effect of LiPSs, the problems of insulative nature of S/Li_2S and the huge volume change (80%) between S and Li_2S would cause a continuous and rapid capacity fade, and emerge as roadblocks for the development of the S cathode. Remarkable approaches have been proposed to address the intrinsic shortcomings of S cathode toward practical applications, including optimization the

Received 10 April 2023; Received in revised form 11 June 2023; Accepted 29 June 2023
Available online 30 June 2023

* Corresponding author, Sen Xin, Tel: (86-10)62568158, E-mail address: xinsen08@iccas.ac.cn.
* Corresponding author, Yu-Guo Guo, Tel: (86-10)82617069, E-mail address: ygguo@iccas.ac.cn.

https://doi.org/10.13208/j.electrochem.2217009

structure of carbon materials, employment of catalysts, utilization of interfacial layer and modification of electrolytes, which are all investigated as important solutions to facilitate conversion kinetics of S cathode [5−10].

Although Li anode shows significant advantages in capacity (3860 $mAh \cdot g^{-1}$) and voltage (−3.042 V) over the conventional graphite anode materials, the generation of Li dendrites and dead Li during Li plating and stripping leads to the formation of unstable SEI and the accompanied low Coulombic efficiency. Hence, the Li metal anode is usually accompanied with serious safety problems and poor cycling performance, which impede the practical application of metal Li-based batteries. Significant efforts have been made to tackle the intrinsic problems of Li anode, including electrolyte additive, artificial SEI, superconcentrated electrolyte and solid-state electrolyte [11−19].

Interestingly, adoption of solid-state electrolyte has been considered as an effective method to restrain the dendrite growth and parasitic reactions on Li anode, but the reports concerning application of solid-state electrolyte on S cathode have less been mentioned [20−23]. Because solid electrolytes are unfavorable to the kinetics of sulfur, whereas liquid electrolytes with higher solubility and mobility of polysulfide could ensure faster redox reaction kinetics of sulfur [24]. Therefore, adopting the asymmetric interfaces which guarantees a liquid environment at S cathode and a solid environment at Li anode could simultaneously facilitate the electrochemical activity of cathode, restrict the shuttling and solve the dendrite problem of anode, and further promotes the advancement of practical Li-S battery.

2. Maintaining reactivity by selecting liquid electrolytes at cathode

The employment of liquid electrolyte at sulfur cathode benefits the solvation of the polysulfide and facilitates the reaction kinetics, but also aggravates the shuttling of polysulfide, which brings about low Coulombic efficiency and short cycling life [25]. The 1,3-dioxolane/1,2-dimethoxyethane (DOL/DME) ether electrolyte, as the most widely used solvent in Li-S batteries, presents moderate solvating capability for polysulfides, good sulfur utilization and fast reaction kinetics. A typical voltage profile with two plateaus of 2.3 V and 2.1 V is observed in DOL/DME-based solutions, which could be illustrated to a general reaction pathway of solid-liquid-solid multi-phase reaction of solid S_8 to soluble S_x^{2-} and finally to solid Li_2S_2/Li_2S [26]. However, for practicable Li-S battery with low E/S ratio (electrolyte/sulfur), several challenges appear in DOL/DME electrolyte, including higher viscosity and lower ionic conductivity, aggravated polysulfide shuttle and electrolyte solution depletion [27−29]. Therefore, other types of electrolyte solutions beyond conventional ether solution should be explored for Li-S cells with better performance.

A series of electrolytes such as high-concentration electrolyte, ionic liquids and hydrofluoroethers solvents have been introduced into Li-S battery. Different from DOL/DME electrolyte, these electrolytes can suppress the dissolution of polysulfides and have limited solubility of Li_2S_8 (from 1 to 100 $mmol \cdot L^{-1}$). Due to different solubilities of polysulfide, the sulfur reaction pathway and electrochemical performance could be significantly changed in comparison to the dissolution-precipitation mechanism in conventional electrolytes.

For high-concentration electrolyte, the interactions between the solvent and salt ions are comparatively stronger than that in 1 $mol \cdot L^{-1}$ electrolyte, forming contact ion pairs (CIP) and aggregates (AGG) instead of plenty of free solvents [30]. Due to the lack of free-state solvent molecules, dissolution of polysulfide is restricted in high-concentration electrolyte, which could resolve the shuttling problem. In addition, high-concentration electrolyte shows other properties, which benefits the charge transfer, electrochemical stability, and battery safety, including high Li^+ transference numbers, wide electrochemical windows and flame retardancy. However, low ionic conductivity and high viscosity are the key issues that restrain the electrochemical performance in cells with high-concentration electrolyte. To solve the problem, diluents with low viscosity could be introduced to form localized high-concentration electrolyte systems [31].

Nazar et al. [32] designed a electrolyte of $(ACN)_2$/LiTFSI with the diluent of a hydrofluorinated (HFE), which could prevent the dissolution of polysulphide in the electrolyte, and ammeliorate the common problems of poor Coulombic efficiency and capacity fading in Li-S battery. In contrast to conventional liquid electrolytes with disproportional coordination, this new electrolyte presents a different solvation structure without the existence of free solvent, that Li^+ cations are closely surrounded by two ACN molecules. This structure renders the electrolyte negligible solubility and limits the mobility of polysulfide, which could enhance the sulfur utilization and further the overall electrochemical behavior (Fig. 1a). The ionic conductivity and viscosity of $(ACN)_2$/LiTFSI/HFE are 1.57 $mS \cdot cm^{-1}$ and 8.6 cP, respectively, which approach to those of DOL/DME solution.

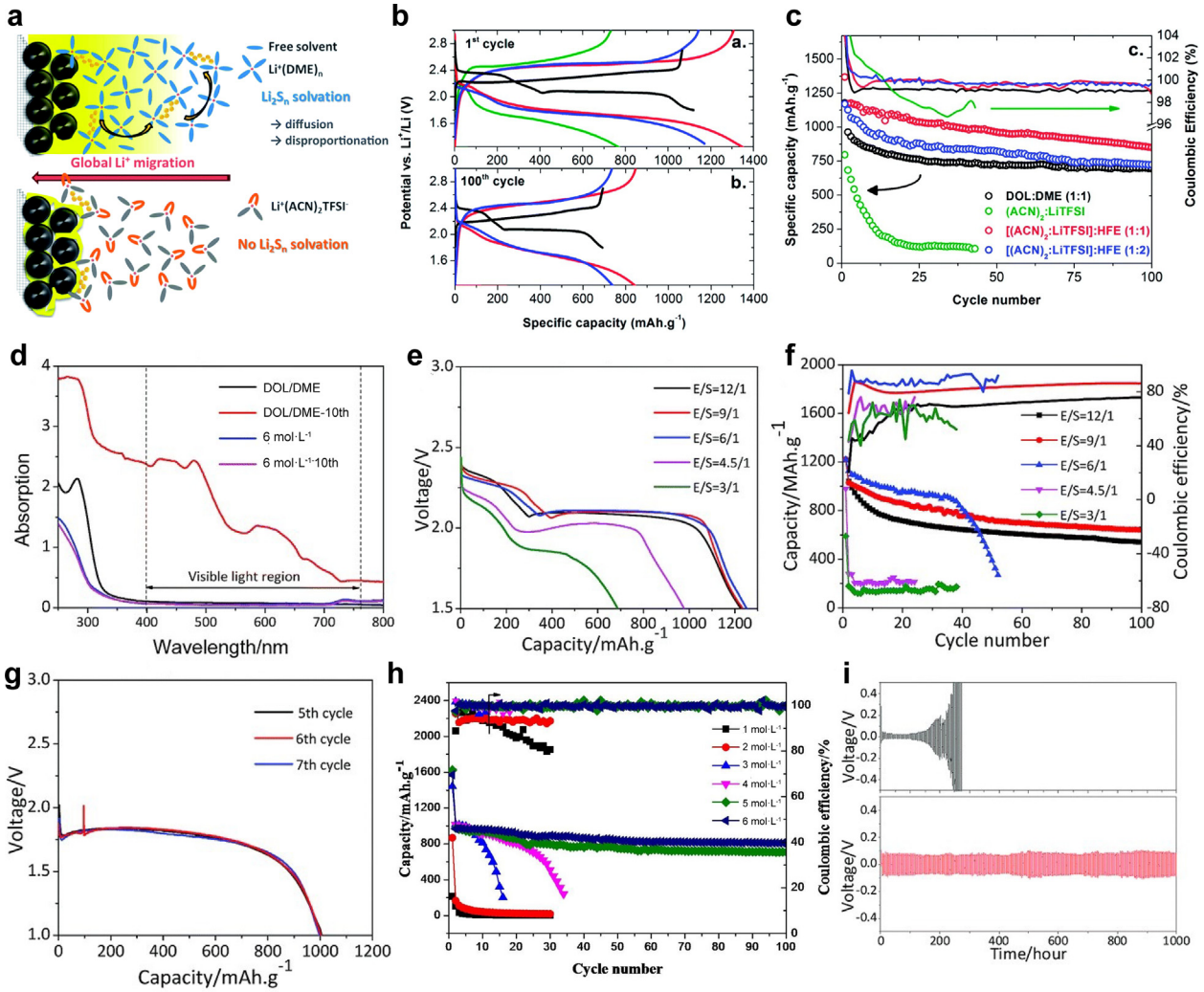

Fig. 1. (a) Schematic illustration of the migration of polysulfides in a Li-S battery with DME electrolyte and $(I)_2$/LiTFSI electrolyte. (b) The initial and 100th galvanostatic discharge curve (GDC) voltage profiles in Li-S batteries at 0.2C with different electrolytes including DOL/DME (black), $(ACN)_2$/LiTFSI (green), ACN/HFE(1:1) (red) aIACN/HFE(1:2) (blue). (c) Cycling performance of different electrolytes in Li-S batteries for 100 cycles. Reproduced with permission of Ref. [32], copyright @ 2014 RSC publishing. (d) UV-vis spectra of various electrolytes from the 10 cycled Li-S batteries. (e–f) GDC voltage profiles of Li-S batteries with varied E/S ratiI(e) in 1 mol·L^{-1} LiTFSI in DOL/DME electrolyte and (f) in HFME-6 mol·L^{-1} carbonate electrolyte at 0.2C. (g) The self-discharge performance of HFME-6 mol·L^{-1} carbonate during the 6th cycle after one-week storage. (h) Cycling performance of Li-S batteries with carbonate electrolyte of different concentrations at 0.2C. (i) Plating-stripping profile of symmetric Li-Li cells in 1 mol·L^{-1} carbonate electrolyte and HFME-6 mol·L^{-1} carbonate electrolyte (1 mA·cm^{-2}, 1 mAh·cm^{-2}). Reproduced with permission of Ref. [33], copyright @ 2013 RSC publishing.

The electrochemical behavior of Li-S battery with $(ACN)_2$/LiTFSI/HFE is distinct from the two-plateau galvanostatic discharge curve in conventional Li-S battery, which shows a sloping curve without any clearly defined plateau (Fig. 1b). Due to the limitation of dissolution and shuttling of polysulfides, the capacity could reach to near the full theoretical capacity of 1373 mAh·g^{-1}, and exhibit a specific capacity of 850 mAh·g^{-1} after 100 cycles at 0.2 C (Fig. 1c). Although the low solubility of polysulfide would lead to cell polarization, the rate performance of Li-S battery with $(ACN)_2$/LiTFSI/HFE is more excellent than that with DOL/DME, which delivers a discharge capacity of 900 mAh·g^{-1} at 1 C.

Carbonate electrolytes have been widely used in lithium-ion batteries or metal lithium batteries but not in Li-S batteries, because they would have serious parasitic reactions with polysulfides. However, when the concentration of lithium salts is high to some extent, the side reactions between carbonate electrolyte and polysulfide could be suppressed [32]. Xiao et al. [33] proposed an ethylene carbonate/diethyl carbonate (EC/DEC) solution with 6 mol·L^{-1} LiTFSI and hexafluoroisopropyl methyl ether (HFME) diluent, which enables the application of carbonate electrolyte in Li-S batteries. Due to high concentration environment of this new electrolyte, almost all carbonate molecules strongly coordinate with Li^+,

which avoids the electrophilic carbon being attacked by polysulfides with high nucleophilic ability. Moreover, the slight amount of dissolved polysulfides would react with the carbonate molecules and form a protection layer on sulfur cathode, which impedes the further side reactions and dissolution of polysulfides. Thus, the high-concentration ester converts the ether-based Li-S batteries from non-rechargeable to rechargeable feature, showing a non-solvent behavior and akin solid-solid conversion. UV-Vis analysis is conducted to investigate the polysulfide solubility in DOL/DME and 6 $mol \cdot L^{-1}$ EC/DEC/LiTFSI electrolytes before and after cycling, which turns out that no polysulfide is generated or solvated during cycling in the 6 $mol \cdot L^{-1}$ EC/DEC/LiTFSI electrolytes (Fig. 1d). Different from the typical two-step voltage profile with dissolution-precipitation process, the 6 $mol \cdot L^{-1}$ EC/DEC/LiTFSI electrolytes shows one-plateau curve and delivers a discharge capacity of 1590 $mAh \cdot g^{-1}$ at 0.2 C. In addition, the Li-S batteries with 6 $mol \cdot L^{-1}$ EC/DEC/LiTFSI electrolytes exhibit superior performance even at low E/S ratios while the batteries with DOL/DME shows high polarization and capacity decay at the E/S ratio less than 5:1 (Fig. 1e–f). This is because at low E/S ratios the transport of ions is influenced by the saturation of polysulfides in DOL/DME electrolyte, but the electrochemical properties of Li-S batteries with 6 $mol \cdot L^{-1}$ EC/DEC/LiTFSI electrolytes only rely on the migration of Li^+ ions. Surprisingly, the Li-S batteries with 6 $mol \cdot L^{-1}$ EC/DEC/LiTFSI electrolytes present a zero self-charge behavior that the galvanostatic discharge curve of a cycled cell ideally remains the same even after one-week storage (Fig. 1g). In view of the property, a brilliant cycling performance is observed that the capacity retention is 83% after 100 cycles and the Coloumbic efficiency is close to 100% at a 0.2 C (Fig. 1h). Except for altering the sulfur reaction mechanism and preventing polysulfides, the high-concentration electrolyte could stably match the metal lithium anode. While the symmetric Li-Li cell with DOL/DME electrolyte presents a huge polarization after 150 h, and the cell with 6 $mol \cdot L^{-1}$ EC/DEC/LiTFSI electrolyte could be cycled over 1000 h without significant voltage fluctuation or dendrite formation (Fig. 1i).

To achieve lower E/S ratio, a class of electrolytes with high-donor number (DN) or high-dielectric constant (ϵ) is adopted, which promotes the solubility of polysulfides and utilization of sulfur, such as dimethyl sulfoxide (DMA), dimethyl sulfoxide (DMSO), and 1-methylimidazole (MeIm) [34]. To model the solution environment in Li-S cells with high specific capacities, 0.1×10^{-3} $mol \cdot L^{-1}$ and 1.6 $mol \cdot L^{-1}$ Li_2S_6 were added into four electrolytes to investigate the polysulfide solubility (Fig. 2a). In contrast to DOL/DME with insoluble residue at the bottom of bottles, DMA, DMSO and MeIm electrolytes could completely dissolve 1.6 $mol \cdot L^{-1}$ Li_2S_6, since highly polarizable solvent endows higher solubility for Li_2S_x species ($x = 2,3,4,6,8$) than DOL/DME electrolytes. As for the electrolytes with 1.6 $mol \cdot L^{-1}$ Li_2S_6, the DMA and DMSO electrolytes show a clear blue color, which implies that S_3^- radical is the predominant species at low concentrations. The UV-Vis spectra also verify the high intensity of S_3^- radical in high DMA, DMSO and Meln electrolytes (Fig. 2b). Whereas, the spectrum of DOL/DME electrolytes does not show the existence of S_3^- but a higher content of S_4^{2-}, indicative a different reduction pathway with high-DN electrolytes. This is because the S_3^- radical as a highly active intermediate could only be stabilized by high-DN electrolytes, and S_3^- radical creates a reaction pathway different from the pathway of S_4^{2-} in conventional electrolytes (Fig. 2c). According to reported study, the dissociation of S_6^{2-} to S_3^- is more preferable in high-DN electrolytes, and S_3^- could retard the surface passivation from solid Li_2S and accelerate the full output of capacity (Fig. 2d). For the sulfur cathode of 2 $mg \cdot cm^{-2}$, Li-S batteries with DMA and DMSO deliver an initial capacity of 1250 $mAh \cdot g^{-1}$ while a cell with DME presents a capacity of 1100 $mAh \cdot g^{-1}$ (Fig. 2e). When the loading amount of sulfur cathode is amplified to 6 $mg \cdot cm^{-2}$, the superiority of cell with DMA than cell with DME is more obvious (Fig. 2f). For batteries with DMSO or Melm, the instability towards metal lithium anode is the key factor for bad electrochemical performance. Zhang et al. [35] proposed a high-DN electrolyte of tetramethylurea (TMU), which could simultaneously stabilize S_3^- and be compatible with metal lithium anode. The TMU/DOL electrolyte shows a high solubility of both Li_2S_8 and Li_2S_4, while Li_2S_4 is hardly dissolved in the DOL/DME electrolyte (Fig. 2g). The electrodeposition kinetics of lithium sulfide (Li_2S) in TMU/DOL and DOL/DME electrolytes is also vastly different by chronoamperometric test. The different peaks in TMU/DOL could be explained by the reduction of S_3^-, which facilitates the deposition of Li_2S with smaller nucleus size and larger nucleation density (Fig. 2h) [36,37]. Equipping with carbon nanotube (CNT)/S composite cathode, Li-S battery with TMU realizes an initial discharge capacity of 1134 $mAh \cdot g^{-1}$ with Couloumbic efficiency over 98% at 0.1C (Fig. 2i). Compared to the capacity of DME cell (943 $mAh \cdot g^{-1}$), the advantage of TMU cell is

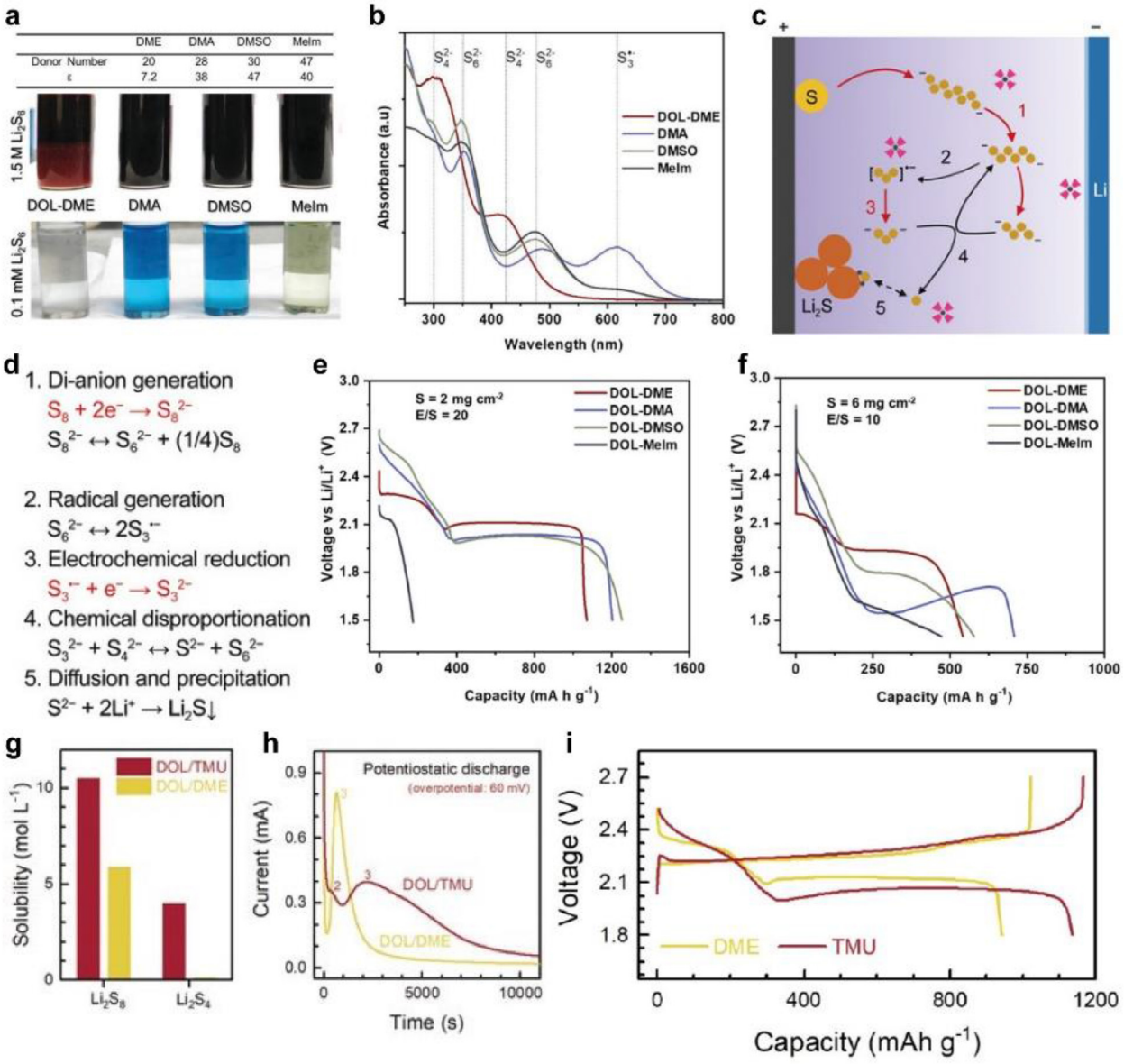

Fig. 2. (a) The table of DN and dielectric constant (ϵ) of the different solvents and optical images of solvents with 1.5 mol·L^{-1} and 0.1 × 10^{-3} mol·L^{-1} Li_2S_6. (b) UV-Vis spectra of DOL-DME, DMA, DMSO, and MeIm electrolytes with 0.25 mol·L^{-1} Li_2S_6. Reproduced with permission of Ref. [34], copyright @ 2018 WILEY-VCH Verlag GmbH & Co. KGaA, Weinheim. (c) Schematic illustration of the sulfur reaction pathway in a TMU-based electrolyte (Arrows: red solid: electrochemical reduction; black solid: chemical dissociation of S_6^{2-} into S_3^{-}; black dashed: equilibrium of dissolution/precipitation). (d) polysulfide reaction pathway proposed by Cuisinier et al. Reproduced with permission of Ref. [35], copyright @ 2018 WILEY-VCH Verlag GmbH & Co. KGaA, Weinheim. (e–f) First cycle discharge profiles with four different electrolytes and (e) 2 mg·cm^{-2} and (f) 6 mg·cm^{-2} sulfur cathode [34]. Reproduced with permission of Ref. [34], copyright @ 2018 WILEY-VCH Verlag GmbH & Co. KGaA, Weinheim. (g) Solubility plots of Li_2S_8 and Li_2S_4 in DOL/TMU vs. in DOL/DME. (h) Chronoamperometric profiles in DOL/DME and DOL/TMU electrolytes. (i) Galvanostatic discharge-charge profiles of Li|CNT/S coin cells at 0.1 C in DME and TMU based electrolytes. Reproduced with permission of Ref. [35], copyright @ 2018 WILEY-VCH Verlag GmbH & Co. KGaA, Weinheim.

reflected by the longer second plateau, which is attributed to an optimal pathway for Li_2S solvation and precipitation.

3. Restraining shuttling by introducing polymer electrolyte as blocking interlayer

Although the adoption of liquid electrolyte guarantees the electrochemical reactivity of sulfur cathode, the shuttling of polysulfide and corrosion of lithium anode would pose challenges for the cycling performance of Li-S battery [38,39]. Therefore, introduction of polymer electrolyte as blocking interlayer could be effective solution. Ding et al. [40] designed a gel polymer electrolyte (GPE) composed of polyvinylidene fluoride (PVDF) and organo-polysulfide polymer (PSPEG), which could be permselective to Li^+ and against

polysulfides. Sun et al. [41] proposed a conductive polypyrrole-coated Celgard, which could simultaneously immobilize polysulfides, and facilitate electron transportation and redox reactions on sulfur cathode. However, these strategies are based on an *ex-situ* synthesis, which results in an inferior interfacial contact between electrolyte and electrodes. Wang et al. [42] mentioned a strategy of gradient solidification, which could ensure a liquid environment at the sulfur cathode with rapid kinetics and an *in-situ* polymerized interface to suppress the shuttling. The solidifying interface is prepared by *in-situ* polymerization of DOL, which is initiated by the $LiPF_6$ loaded on one side of the commercial PE separator towards the S cathode (Fig. 3a). During the battery assembly, the injected ether liquid electrolyte flows through the $LiPF_6$ layer on the separator and triggers gelation of the electrolyte. Due to the slow diffusion in the gel electrolyte, the concentration of dissolved $LiPF_6$ continuous to be declined from the separator to the cathode surface and to the bulk of the cathode, which accounts for different polymerization degrees of DOL. As a result, a thin gradient solidification layer forms at the cathode/electrolyte interface (Fig. 3b). The liquid electrolyte is maintained in the bulk of cathode to enable wetting of S by liquid electrolyte for high electrochemical activity. On the other hand, the surface of separator is highly solidified, which effectively inhibits the dissolution and shuttle of polysulfides, and improves the cycling performance of cell. The chemical species along the gel electrolyte were detected and visualized by time-of-flight secondary ion mass spectrometry (ToF-SIMS), showing a continuous increment of the Li^-, F^-, and P^- signals from the surface (at the cathode side) to the bulk of the gel (Fig. 3c). According to the intensity of representative signals, the concentration in the bulk of gel electrolyte is 1.5 $mol \cdot L^{-1}$ and the concentration of the gel surface is around 0.15 $mol \cdot L^{-1}$, implies that only a minute amount of salt could reach the bulk of the cathode and cannot introduce the gelation process (Fig. 3d). As shown in Fig. 4G–H, the prepared $LiPF_6$-supported separator strips could be easily rolled up without

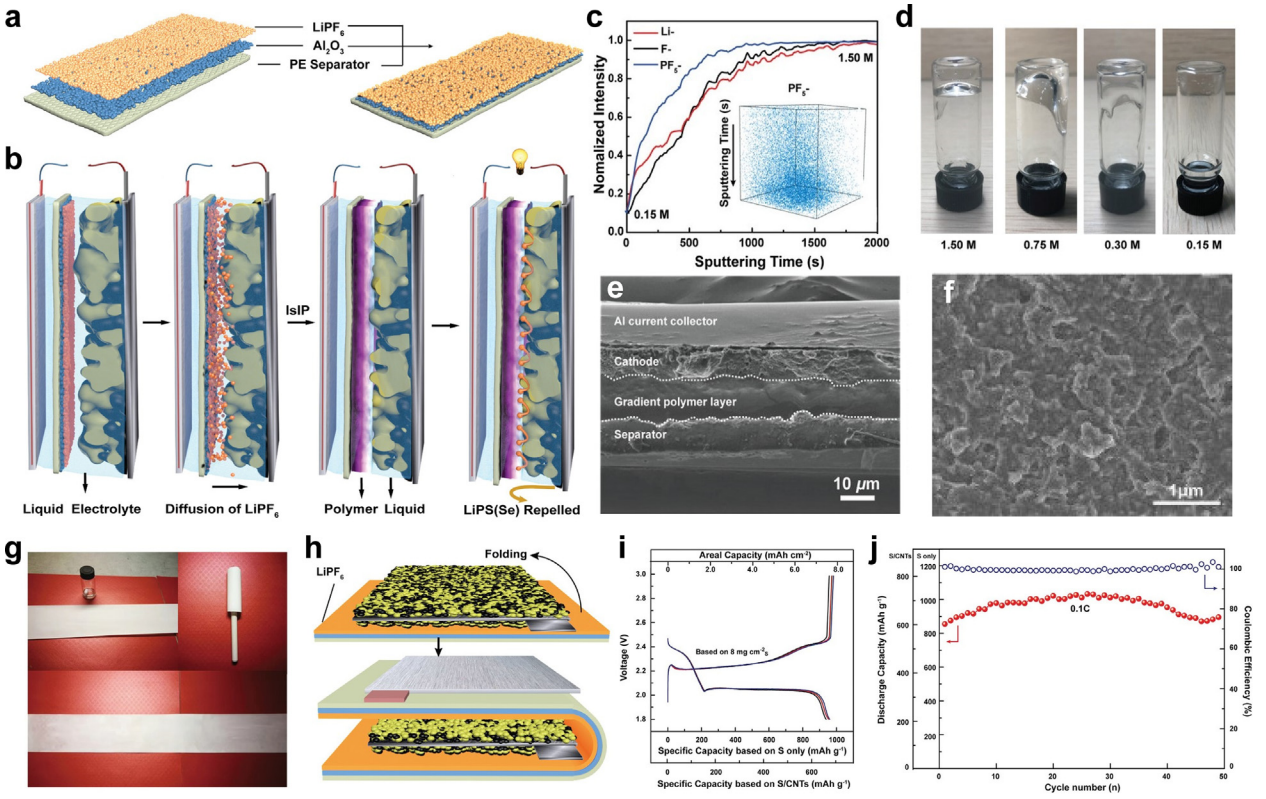

Fig. 3. (a) Structure of the $LiPF_6/Al_2O_3$/PE separator. (b) Schematic illustration showing the in-situ interfacial polymerization of liquid electrolyte realized with the $LiPF_6/Al_2O_3$/PE separator. (c) TOF-SIMS depth profiles obtained from the gel polymer interlayer on the separator, in which the inset shows the 3D spatial configuration of PF_5 signal. (d) Optical images showing the various polymerization degrees of liquid electrolyte with different $LiPF_6$ concentrations. (e) Cross-sectional SEM image illustrating multilayered structure of the Li-S full battery. (f) SEM image of sulfur cathode surface after the polymerization having been finished. (g) Optical images showing the preparation process of the $LiPF_6/Al_2O_3$/PE separator roll. (h) Schematic illustration of the steps for the assembly of Li-S pouch cells. (i) GDC voltage profiles and (j) cycling performance of the assembled Li-S pouch cell at 0.1C. Reproduced with permission of Ref. [42], copyright @ 2020 WILEY-VCH Verlag GmbH & Co. KGaA, Weinheim.

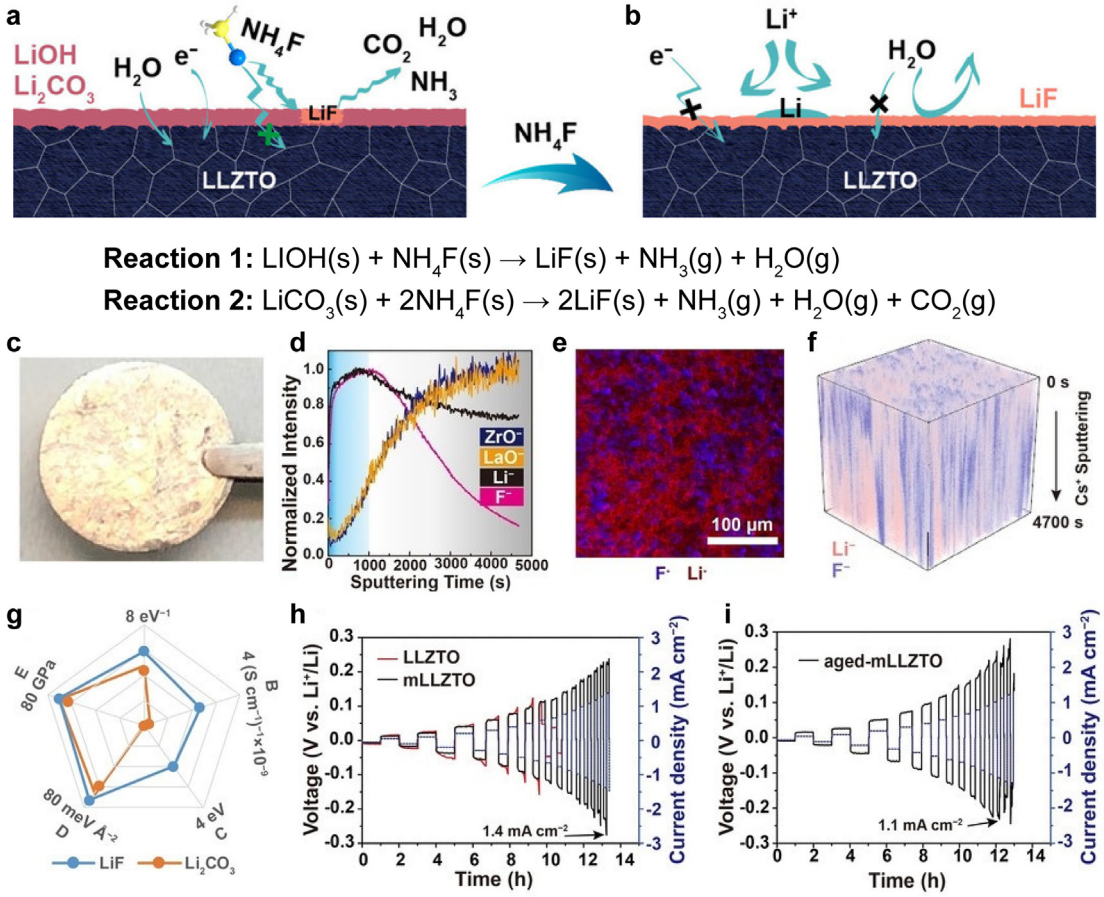

Fig. 4. (a) Schematic illustration showing the formation of LiF-coated LLZTO by NH_4F treatment. (b) The surface stability of LiF-coated LLZO against air exposure, electron and hostless evolution of Li metal; (c) Optical image of the wetting behavior of molten Li on mLLZTO. (d) Depth profiles of ZrO^-, LaO^-, Li^- and F^- signals at the Li/mLLZTO interface. High-resolution (e) 2D/ (f) 3D maps of Li^- and F^-signals at the Li/mLLZTO interface. (g) Comparation of LiF and Li_2CO_3 in various physical and chemical properties; A: 1/surface diffusion barrier energy; B: 1/electronic conductivity; C: electron tunnelling barrier; D: interfacial energy; E: bulk modulus. (h) Galvanostatic Li plating/stripping voltage profiles at step-increased current densities of Li/Li symmetric cells assembled with the LLZTO and mLLZTO pellets. (i) Galvanostatic Li plating/stripping voltage profiles at step-increased current densities of Li/Li symmetric cells assembled with the mLLZTO pellets after being aged in the air for 2 days. Reproduced with permission of Ref. [50], copyright @ 2020 WILEY-VCH Verlag GmbH & Co. KGaA, Weinheim.

any exfoliation of $LiPF_6$ powder and the pouch cell adopted a typical "Z stacking" configuration. The battery with new separator delivers a high initial capacity of 1100 $mAh \cdot g^{-1}$ and a reversible capacity of 1000 $mAh \cdot g^{-1}$ at 0.1C, and a reversible capacity of around 900 $mAh \cdot g^{-1}$ at 0.5C, even at a high S mass content of 70%. By using the strategy, a practical Li-S pouch cell was assembled, which delivered a high reversible capacity of 950 $mAh \cdot g^{-1}$ and a lifespan of 50 cycles at a high S mass loading of 8 $mg \cdot cm^{-2}$ (Fig. 3i–j).

4. Suppressing dendrites by adopting solid-state electrolytes at anode

To address the dendrite issue in Li-metal batteries, ceramic solid electrolytes, such as cubic garnet-type LLZO or its derivatives, have been regarded as one of the most promising solutions [43–46]. It simultaneously features many advantages, including high Li^+ conductivity, high Li^+ transference number, wide electrochemical window of 0–6 V, and high shear modulus and high compactness, which are beneficial to inhibit dendrite evolution and stabilize the Li/electrolyte interface. However, the garnet itself shows poor chemical stability against water and carbon dioxide in the ambient air. Once been exposed in the air, many Li-containing contaminants, including lithium hydroxide and Lithium carbonate, would be generated on the garnet surface, which show low Li-ion conductivity and poor wettability against Li metal (Fig. 4a). Thus, these surface contaminants may easily trigger dendrite nucleation and formation at the interface, so they are supposed to be removed by strong acid or high-temperature sintering [47–49].

To improve the chemical stability against air exposure, Duan et al. [50] developed a simple and moderate-temperature chemistry to convert the contaminants into a fluorinated nanocoating layer on the surface of the garnet particles (Fig. 4b). According to the theory that ammonia fluoride is capable to react with lithium hydroxide and lithium carbonate, the LiF-coated garnet-type LLZTO pellets were prepared by the treatment with NH_4F. The treated LLZTO pellet was not contaminated even after being aged in ambient air for a few days. This is because of the hydrophobic nature from the fluorinated garnet surface, which prevents the contaminant-generating parasitic reactions between LLZTO and moist in the air. By being dipped into molten Li, a uniform garnet layer could intimately coat on the surface of Li metal (Fig. 4c). TOP-SIMS results show that the ZrO^- and LaO^- signals representing the LLZTO are gradually increased, but the F^- signal firstly remains stable and later quickly diminishes (Fig. 4d). With the proof of 2D and 3D configurations of F^- and Li^- signals, it can be seen that LiF nanocoating on mLLZTO remains stable during the formation of Li/garnet interface.

Considering that LiF has a lower barrier energy for diffusion of Li^+ on the surface (0.17 eV) and a higher electron tunnelling barrier (2 eV) than those of Li_2CO_3 (0.23 eV and 0 eV, respectively), the fluorinated interface helps to form smooth and compact deposits rather than typically rough and dendritic morphology even at high current densities (Fig. 4g). In addition, the Li^+ diffusivity at an electrode/electrolyte interface plays a key role in controlling the critical current density, so that the modified interface could enable the regulated Li plating/stripping at a high Li^+ flux and achieve a prolonged cycling of Li/Li symmetric cells at a high critical current density of 1.4 $mA\cdot cm^{-2}$ (Fig. 4h). After air exposure, the LLZTO pellet still keeps high critical current density of 1.1 $mA\cdot cm^{-2}$ (Fig. 4i).

Although the adoption of garnet electrolyte could suppress the Li dendrite, it is difficult to apply conventional manufacture techniques to prepare ceramic oxide electrolyte pellets with thickness of <200 μm due to the inherently brittle nature of garnet electrolyte property. Furthermore, the ceramic pellet does not have adequate "softness" to accommodate the deformation strains caused by the volume change of electrode materials during Li^+ plating/stripping. Nevertheless, the garnet powder does not support fast interparticle Li^+ conduction at loosely-packed grain/particle boundaries. Therefore, adopting solid composite electrolytes especially with thin-film polymer could be effective solution towards the pathway to a practical solid-state Li-metal battery [46,51].

Chen et al. [52] introduced a uniform polyacrylonitrile nanocoating on the surface of LLZTO garnet particles by high-energy ball-milling. The cross-sectional SEM image shows that the total thickness of the solid electrolyte layer is < 10 μm (LLZTO@PAN 8 μm and PEO 1 μm), which meets the requirements for building LMBs with competitive energy density (Fig. 5a). It is also noted that the LLZTO@PAN particles could permeate into both the LFP layer and the PEO electrolyte layer, which is beneficial for facilitating Li^+ conduction at heterointerfaces. The modified garnet powder shows an ultrahigh mass content of ceramics of 94.3% and a polymer coating with a thickness of 7 nm, which ensures efficient interparticle Li^+ transport without pellet sintering or applying external pressure. According to the FTIR and NMR spectra, the coupling between DMSO and LLZTO leads to dehydrocyanation of PAN on the garnet surface and formation of conjugated structures in the polymer phase. According to DFT calculations, dehydrocyanated PAN shows enhanced interaction with the garnet surface with strong electron transfer, and a space charge layer is formed at the garnet/polymer interface, which contributes to faster interfacial Li^+ exchange. In addition, because the thickness of the polymer coating falls into the same scale as the space charge layer and the conjugated region, Li ions are easily and rapidly transported between two adjacent ceramic particles through the polymer phase (Fig. 5b). The interparticle lithium conduction mechanism is further testified by solid-state NMR measurement. The 2D $^1H-^7Li$ heteronuclear correlation spectrum indicates that the Li ions dissociated from LiTFSI are trapped by the C=C bond possibly because of the high electron density (Fig. 5c). Meanwhile, 2D $^7Li-^7Li$ exchange spectrum indicates fast Li $^+$ exchange at the garnet/polymer interface (Fig. 5d). With PAN providing the Li^+ transport channels between the garnet particles, thin-film electrolytes with a thickness of less than 10 μm can be prepared from the LLZTO@PAN powder via tape-casting directly on the cathode surface. The composite solid electrolyte exhibits a high ionic conductivity of 1.1×10^{-4} $S\cdot cm^{-1}$ at 60 °C with an activation energy of 0.36 eV, indicating an improved wetting of PAN on LLZTO and a low energy barrier for Li^+ diffusion (Fig. 5e). Also, the electrolyte presents a high Li^+ transference number of 0.66, which is favorable for restricting the growth of dendrite during the plating/stripping of Li metal (Fig. 5f). Assembled with the electrolyte, the Li/LFP all-

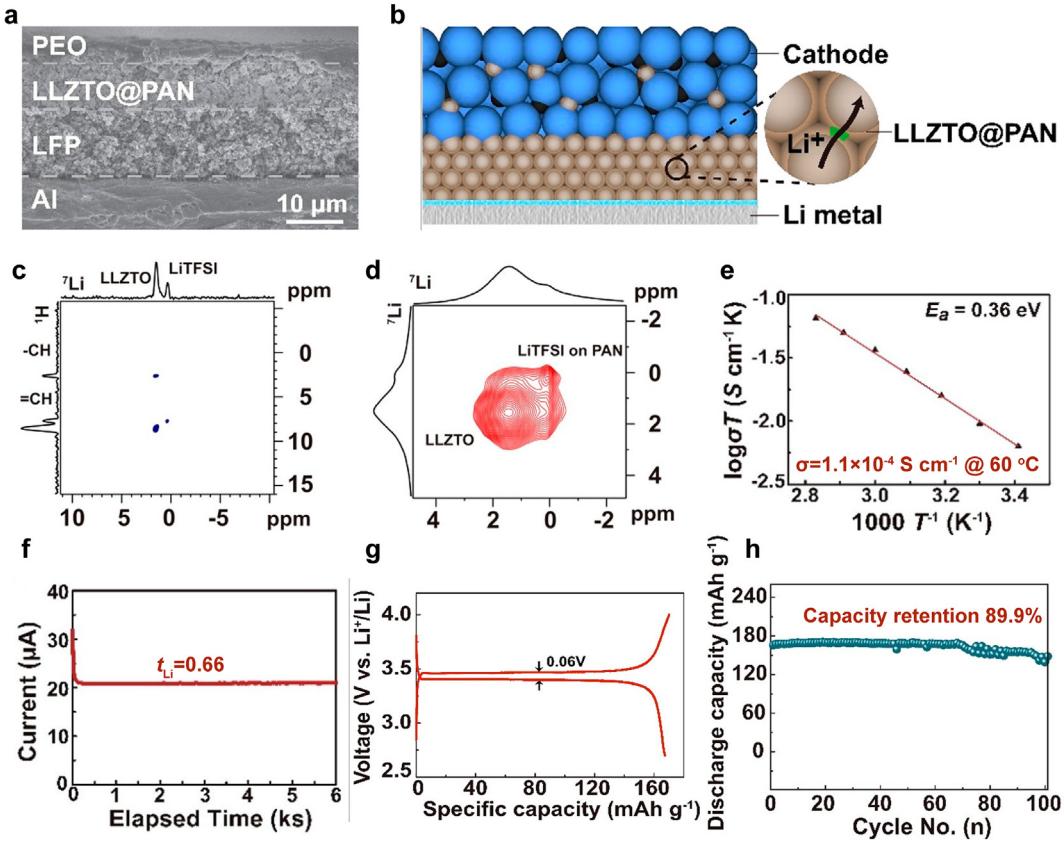

Fig. 5. (a) Cross-sectional SEM image LLZTO@PAN and PEO electrolyte layers on the cathode; (b) Schematics showing different Li^+ transport mechanisms through the ceramics/polymer interface; (c) 2D Solid-state NMR $^7Li-^1H$ HETCOR spectra of LLZTO@PAN at 298 K. (d) 2D Solid-state NMR $^7Li-^7Li$ HETCOR spectra of LLZTO@PAN at 298 K. (e) Arrhenius plot of LLZTO@PAN at varied temperatures; (f) Chronoamperometric profile of a symmetric Li/Li cell with the LLZTO@PAN electrolyte; (g) Charge-discharge voltage profile at 0.1C of Li/LFP cell with the LLZTO@PAN electrolyte (h) Cycling performance of the Li//LLZTO@PAN/PEO//LFP cell at 60 °C at 0.1C. Reproduced with permission of Ref. [51], copyright @ 2021 American Chemical Society.

solid-state cell delivers a high reversible capacity of 167 $mAh \cdot g^{-1}$ at 0.1C with a small polarization of 0.06 V (Fig. 5g), and achieves a capacity retention of 89.6% after 100 cycles (Fig. 5h).

In addition to oxide electrolytes, sulfide electrolytes and organic-inorganic composite electrolytes have also been used to suppress Li dendrites. Wang et al. [53] improved the interfacial contact and charge transfer stability between sulfide electrolyte and Li metal anode by applying a LiF-rich *in-situ* solidified Li^+-conductive interlayer, leading to inhibition of electrolyte decomposition and dendrite-free Li plating/stripping at the interface. Chen et al. [54] designed a composite electrolyte with fast ion-conducting ceramic nanofiller and functional polymer skeleton, which enable a dendrite-free Li surface after cycling.

5. Conclusions

For practical application of Li-S batteries, a series of problems should be solved, including the dissolution/shuttle of LiPSs, the sluggish interfacial charge transfer, the damage of cathode bulk structure and uncontrollable Li dendrite growth. In view of different situations at cathode and anode sides, asymmetric electrode/electrolyte interfaces should be constructed. To conclude, this review discusses types of strategies at cathode, separator and anode sides in the Li-S battery. From a practical point of view, an ideal Li-S battery should take into account high energy density and long cycle life, which requires that the electrolyte could optimize the electrochemical reactivity of sulfur, prevent the shuttling of polysulfide and stabilize the metal lithium anode. Accordingly, a liquid electrolyte should be used inside cathode to ensure fast Li^+ transport, a gel electrolyte should be used on cathode side to achieve good interfacial contact and inhibit polysulfide shuttle, and a solid-state electrolyte should be used on anode side to suppress Li dendrites. By purposely selecting suitable strategies at the corresponding domain and building asymmetric interfaces, we would obtain a high-performance and practical Li-S battery.

Acknowledgements

This work was supported by the National Key R&D Program of China (Grant No. 2019YFA0705703), CAS Project for Young Scientists in Basic Research (Grant No. YSBR-058), the National Natural Science Foundation of China (Grant Nos. 21975266, 52172252 and 22209188), and the Beijing Natural Science Foundation (Grant No. JQ22005).

References

[1] Seh Z W, Sun Y, Zhang Q, Cui Y. Designing high-energy lithium-sulfur batteries[J]. Chem. Soc. Rev., 2016, 45(20): 5605−5634.

[2] Xu H H, Wang S F, Manthiram A. Hybrid lithium-sulfur batteries with an advanced gel cathode and stabilized lithium-metal anode[J]. Adv. Energy Mater., 2018, 8(23): 1800813.

[3] Wang L L, Ye Y S, Chen N, Huang Y X, Li L, Wu F, Chen R J. Development and challenges of functional electrolytes for high-performance lithium-sulfur batteries[J]. Adv. Funct. Mater., 2018, 28(38): 1800919.

[4] Peng H J, Huang J Q, Cheng X B, Zhang Q. Review on high-loading and high-energy lithium-sulfur batteries[J]. Adv. Energy Mater., 2017, 7(24): 1700260.

[5] Huang S, Guan R T, Wang S J, Xiao M, Han D M, Sun L Y, Meng Y Z. Polymers for high performance Li-S batteries: material selection and structure design[J]. Prog. Polym. Sci., 2018, 89: 19−60.

[6] Barghamadi M, Best A S, Bhatt A I, Hollenkamp A F, Ruether T. Lithium-sulfur batteries —the solution is in the electrolyte, but is the electrolyte a solution?[J]. Energy Environ. Sci., 2014, 7(12): 3902−3920.

[7] Yan M, Wang W P, Yin Y X, Wan L J, Guo Y G. Interfacial design for lithium-sulfur batteries: from liquid to solid[J]. Energy Chem., 2019, 1(1): 100002.

[8] Nazar L F, Cuisinier M, Quan P. Lithium-sulfur batteries[J]. MRS Bull, 2014, 39(5): 436−442.

[9] Li W, Wang P, Zhang M, Pan H, He X W, He P, Zhou H S. Functional CNTs@EMIM$^+$-Br$^-$ electrode enabling polysulfides confining and deposition regulating for solid-state Li-sulfur battery[J]. Small, 2023, 19(6): 2205809.

[10] Wang P F, He X, Lv Z C, Song S, Song X, Yi T F, Xu N, He P, Zhou H S. Light-driven polymer-based all-solid-state lithium-sulfur battery operating at room temperature[J]. Adv. Funct. Mater., 2023, 33(5): 2211074.

[11] Guo Y P, Li H Q, Zhai T Y. Reviving lithium-metal anodes for next-generation high-energy batteries[J]. Adv. Mater., 2017, 29(29): 1700007.

[12] Cheng X B, Zhang R, Zhao C Z, Zhang Q. Toward safe lithium metal anode in rechargeable batteries: a review[J]. Chem. Rev., 2017, 117(15): 10403−10473.

[13] Xin S, Chang Z W, Zhang X B, Guo Y G. Progress of rechargeable lithium metal batteries based on conversion reactions[J]. Natl. Sci. Rev., 2017, 4(1): 54−70.

[14] Zhang R, Li N W, Cheng X B, Yin Y X, Zhang Q, Guo Y G. Advanced micro/nanostructures for lithium metal anodes [J]. Adv. Sci., 2017, 4(3): 1600445.

[15] Xin S, You Y, Wang S, Gao H, Yin Y X, Guo Y G. Solid-state lithium metal batteries promoted by nanotechnology: progress and prospects[J]. ACS Energy Lett., 2017, 2(6): 1385−1394.

[16] Lu D, Shao Y, Lozano T, Bennett W D, Graff G L, Polzin B, Zhang J, Engelhard M H, Saenz N T, Henderson W A. Failure mechanism for fast-charged lithium metal batteries with liquid electrolytes[J]. Adv. Energy Mater., 2015, 5(3): 1400993.

[17] Cheng X B, Zhang R, Zhao C Z, Wei F, Zhang J G, Zhang Q. A review of solid electrolyte interphases on lithium metal anode[J]. Adv. Sci., 2016, 3(3): 1500213.

[18] Yasin G, Arif M, Mehtab T, Lu X, Yu D L, Muhammad N, Nazir M T, Song H H. Understanding and suppression strategies toward stable Li metal anode for safe lithium batteries[J]. Energy Storage Mater., 2020, 25: 644−678.

[19] Pan H, Zhang M H, Cheng Z, Jiang H Y, Yang J G, Wang P F, He P, Zhou H S. Carbon-free and binder-free Li-Al alloy anode enabling an all-solid-state Li-S battery with high energy and stability[J]. Sci. Adv., 2022, 8(15): eabn4372.

[20] Kalaga K, Rodrigues M, Gullapalli H, Babu G, Ajayan P M. Quasi-solid electrolytes for high temperature lithium ion batteries[J]. ACS Appl. Mater. Inter., 2015, 7(46): 25777.

[21] Markevich E, Salitra G, Rosenman A, Talyosef Y, Chesneau F, Aurbach D. The effect of a solid electrolyte interphase on the mechanism of operation of lithium-sulfur batteries[J]. J. Mater. Chem. A, 2015, 3(39): 19873−19883.

[22] Markevich E, Salitra G, Talyosef Y, Chesneau F, Aurbach D. Review—on the mechanism of quasi-solid-state lithiation of sulfur encapsulated in microporous carbons: is the existence of small sulfur molecules necessary? [J]. J. Electrochem. Soc., 2017, 164: A6244−A6253.

[23] Hassoun J, Scrosati B. Moving to a solid-state configuration: a valid approach to making lithium-sulfur batteries viable for practical applications[J]. Adv. Mater., 2010, 22(45): 5198.

[24] Yu X, Manthiram A. Electrode-electrolyte interfaces in lithium-sulfur batteries with liquid or inorganic solid electrolytes[J]. Accounts Chem. Res., 2017, 50(11): 2653−2660.

[25] Liu Y, Elias Y, Meng J, Aurbach D, Pang Q. Electrolyte solutions design for lithium-sulfur batteries[J]. Joule, 2021, 5(9): 2323−2364.

[26] Hou L P, Zhang X Q, Li B Q, Zhang Q. Challenges and promises of lithium metal anode by soluble polysulfides in practical lithium-sulfur batteries[J]. Mater. Today, 2021, 45: 62.

[27] Zhao M, Li B Q, Zhang X Q, Huang J Q, Zhang Q. A perspective toward practical lithium-sulfur batteries[J]. ACS Central Sci., 2020, 6(7): 1095.

[28] Bhargav A, He J, Gupta A, Manthiram A. Lithium-sulfur batteries: attaining the critical metrics[J]. Joule, 2020, 4(2): 285−291.

[29] Zhao M, Li B Q, Peng H J, Yuan H, Huang J Q. Challenges and opportunities towards practical lithium-sulfur batteries under lean electrolyte conditions[J]. Angew. Chem. Int. Ed., 2019, 132(31): 2−20.

[30] Yama Da Y, Wang J H, Ko S, Watanabe E, Yamada A. Advances and issues in developing salt-concentrated battery electrolytes[J]. Nat. Energy, 2019, 4(4): 269−280.

[31] Chen S R, Zheng J M, Mei D H, Han K S, Engelhard M H, Zhao W G, Xu W, Liu J, Zhang J G. High-voltage lithium-metal batteries enabled by localized high-concentration electrolytes[J]. Adv. Mater., 2018, 30(21): 1706102.

[32] Cuisinier M, Cabelguen P E, Adams B D, Garsuch A, Balasubramanian M, Nazar L F. Unique behaviour of nonsolvents for polysulphides in lithium-sulphur batteries [J]. Energy Environ. Sci., 2014, 7(8): 2697−2750.

[33] Huang F F, Gao L J, Zou Y P, Ma G Q, Zhang J J, Xu S Q, Li Z X, Liang X. Akin solid-solid biphasic conversion Li-S battery revealed by coordinated carbonate electrolyte[J]. J. Mater. Chem. A., 2019, 7(20): 12498−12506.

[34] Gupta A, Bhargav A, Manthiram A. Highly solvating electrolytes for lithium-sulfur batteries[J]. Adv. Energy Mater., 2019, 9(6): 1803096.

[35] Zhang G, Peng H J, Zhao C Z, Chen X, Zhao L D, Li P, Huang J Q, Zhang Q. The radical pathway based on a lithium-metal-compatible high-dielectric electrolyte for lithium-sulfur batteries[J]. Angew. Chem. Int. Ed., 2018, 57(51): 16732.

[36] Cuisinier M, Hart C, Balasubramanian M, Garsuch A, Nazar L F. Radical or not radical: revisiting lithium-sulfur electrochemistry in nonaqueous electrolytes[J]. Adv. Energy Mater., 2015, 5(16): 1401801.
[37] Zou Q, Lu Y C. Solvent-dictated lithium sulfur redox reactions: an operando UV-vis spectroscopic study[J]. J. Phys. Chem. Lett., 2016, 7(8): 1518.
[38] Wang W P, Zhang J, Chou J, Yin Y X, You Y, Xin S, Guo Y G. Solidifying cathode-electrolyte interface for lithium-sulfur batteries[J]. Adv. Energy Mater., 2021, 11(2): 2000791.
[39] Liu F Q, Wang W P, Yin Y X, Zhang S F, Guo Y G. Upgrading traditional liquid electrolyte via *in situ* gelation for future lithium metal batteries[J]. Sci. Adv., 2018, 4(10): eaat5383.
[40] Shen Y Q, Zeng F L, Zhou X Y, Wang A B, Wang W K, Yuan N Y, Ding J N. A novel permselective organo-polysulfides/PVDF gel polymer electrolyte enables stable lithium anode for lithium-sulfur batteries[J]. J. Energy Chem., 2020, 48: 267−276.
[41] Li Y J, Wang W Y, Liu X X, Mao E Y, Wang M T, Li G C, Fu L, Li Z, Eng A YS, She Z W, Sun Y M. Engineering stable electrode-separator interfaces with ultrathin conductive polymer layer for high-energy-density Li-S batteries[J]. Energy Storage Mater., 2019, 23: 261−268.
[42] Wang W P, Zhang J, Yin Y X, Duan H, Chou J, Li S Y, Yan M, Xin S, Guo Y G. A rational reconfiguration of electrolyte for high-energy and long-life lithium-chalcogen batteries[J]. Adv. Mater., 2020, 32(23): 2000302.
[43] Fu K K, Gong Y, Hitz G T, McOwen D W, Li Y, Xu S, Wen Y, Zhang L, Wang C, Pastel G. Three-dimensional bilayer garnet solid electrolyte based high energy density lithium metal-sulfur batteries[J]. Energy Environ. Sci., 2017, 10(7): 1568.
[44] Wang Q S, Jin J, Wu X W. A shuttle effect free lithium sulfur battery based on a hybrid electrolyte[J]. Phys. Chem. Chem. Phys., 2014, 16(39): 21225−21229.
[45] Wang Q S, Guo J, Wu T, Jin J, Yang J H, Wen Z Y. Improved performance of Li-S battery with hybrid electrolyte by interface modification[J]. Solid State Ion, 2017, 300: 67−72.
[46] Sun C Z, Huang X, Jin J, Lu Y, Wang Q, Yang J H, Wen Z Y. An ion-conductive $Li_{1.5}Al_{0.5}Ge_{1.5}(PO_4)_3$-based composite protective layer for lithium metal anode in lithium-sulfur batteries[J]. J. Power Sources, 2018, 377(15): 36−43.
[47] Ozhabes Y, Gunceler D, Arias T A. Stability and surface diffusion at lithium-electrolyte interphases with connections to dendrite suppression[J]. Physics, 2015: arXiv.1504.05799.
[48] Liu Z, Qi Y, Lin Y X, Chen L, Lu P, Chen L Q. Interfacial study on solid electrolyte interphase at Li metal anode: implication for Li dendrite growth[J]. J. Electrochem. Soc., 2016, 163(3): A592.
[49] Fan X L, Ji X, Han F D, Yue J, Chen J, Chen L, Deng T, Jiang J J, Wang C S. Fluorinated solid electrolyte interphase enables highly reversible solid-state Li metal battery[J]. Sci. Adv., 2018, 4(12): eaau9245.
[50] Duan H, Chen W P, Fan M, Wang W P, Yu L, Tan S J, Chen X, Zhang Q, Xin S, Wan L J, Guo Y G. Building an air stable and lithium deposition regulable garnet interface from moderate-temperature conversion chemistry[J]. Angew. Chem. Int. Ed., 2020, 59(29): 12069.
[51] Fu K, Gong Y H, Dai J Q, Gong A, Han X G, Yao Y G, Wang C W, Wang Y B, Chen Y N, Yan C Y, Li Y J, Wachsman E D, Hu L B. Flexible, solid-state, ion-conducting membrane with 3d garnet nanofiber networks for lithium batteries[J]. PNAS, 2016, 113(26): 7094−7099.
[52] Chen W P, Duan H, Shi J L, Qian Y, Wan J, Zhang X D, Sheng H, Guan B, Wen R, Yin Y X, Xin S, Guo Y G, Wan L J. Bridging interparticle Li^+ conduction in a soft ceramic oxide electrolyte[J]. J. Am. Chem. Soc., 2021, 143(15): 5717.
[53] Wang Y H, Yue J, Wang W P, Chen W P, Zhang Y, Yang Y G, Zhang J, Yin Y X, Zhang X, Xin S, Guo Y G. Constructing a stable interface between the sulfide electrolyte and the Li metal anode via a Li^+-conductive gel polymer interlayer[J]. Mater. Chem. Front., 2021, 5(14): 5328−5335.
[54] Chen H, Zhou C J, Dong X R, Yan M, Liang J Y, Sin S, Wu X W, Guo Y G, Zeng X X. Revealing the superiority of fast ion conductor in composite electrolyte for dendrite-free lithium-metal batteries[J]. ACS Appl. Mater. Interfaces, 2021, 13(19): 22978−22986.

面向高性能锂-硫二次电池应用的非对称电极-电解质界面

丑　佳[a,b]，王雅慧[a,b]，王文鹏[a]，辛　森[a,b,*]，郭玉国[a,b,*]
[a] 中国科学院化学研究所，北京 100190
[b] 中国科学院大学，北京 100049

摘要

锂-硫电池具有高的理论电芯比能量和低成本，是极具应用前景的下一代电化学储能技术，已被广泛研究。实用化锂-硫电池技术目前面临的挑战主要包括正极侧电活性硫物种在充放电过程中的不可逆损失，负极侧枝晶形核生长，以及因活性硫迁移至负极而导致的界面副反应，上述问题会导致电池工况条件下性能迅速衰退，引发电池失效和安全问题。本工作中，我们提出通过设计非对称的电极-电解质界面稳定锂-硫电池正负极电化学，协同促进电极/电解质体相和界面电荷输运，从而延长电池循环寿命，显著提升电化学性能。本文所讨论的策略有望指导电池界面理性设计，助力实现高性能的锂-硫电池。

关键字： 锂-硫电池；锂金属负极；硫正极；电极-电解质界面